X International Conference on Computational Methods in Marine Engineering
MARINE 2023
J. Garcia-Espinosa, L. González, J.E. Gutiérrez & B. Serván-Camas (Editors)

Application of Deep Neural Networks to the Hull Form Optimization of a SWATH Vessel for Improving Its Calm Water Resistance

MARINE 2023

Chi-Min Wu[*], Yu-Tung Lin[†] and Shiu-Wu Chau[†]

[*]Dept. of Eng. Sci. and Ocean Engineering
National Taiwan University
No. 1, Sec. 4, Roosevelt Rd., 10617 Taipei, Taiwan
e-mail: r09525098@ntu.edu.tw

[†]Dept. of Eng. Sci. and Ocean Engineering
National Taiwan University
No. 1, Sec. 4, Roosevelt Rd., 10617 Taipei, Taiwan
e-mail: r10525006@ntu.edu.tw, chausw@ntu.edu.tw

ABSTRACT

This study uses deep neural network (DNN) to optimize the hull form of a small water-plane area twin hull vessel, where two pairs of NACA-shaped fin stabilizers are installed on each pontoon to keep an even keel condition. The vessel's target condition is a speed of 24 knots and a displacement of 120 tons. Four parameters are used to define the pontoon geometry, and a fixed the pontoon length of 22.5 m is adopted. A flow solver, STAR-CCM+, is employed to predict the resistance of the pontoon and fin stabilizer, and Rhinocero3D is used in the parametric pontoon design. About 1400 pontoon designs are used to train the DNN model to correlate the resistance with the design parameters, and 80 cases are adopted for testing, where an improvement of 12.8% in calm-water resistance compared to the baseline design is achieved. The optimized pontoon design has a fore-body of 2 m, an aft-body of 5.71 m, an angle of entrance of 37°, and an angle of run of 19°.

Keywords: Calm Water Resistance; Hull Form Optimization; Deep Neural Network; Pontoon; SWATH.

1. INTRODUCTION

Taiwan's topography is favorable for the development of offshore wind. As more and more offshore wind farms are built and planned (GWEC, 2021), there is an increasing demand for Crew Transfer Vessels (CTVs). This type of vessel requires sufficient stability in waves to ensure the safety and comfort of the crew in wind farm maintenance operations. Small Waterplane Area Twin Hull (SWATH) can easily meet these requirements (Y. Dalgic *et al.*, 2015).

SWATH is composed of the pontoon, which provides the main buoyancy of SWATH, and the strut, which connects the deck and the pontoon and pierces the free surface. Compared with other vessel types, SWATH is well-known for its excellent wave resistance in high wave conditions (S. Brizzolara, *et al*., 2011). However, due to a small waterplane area, SWATH vessels lack longitudinal restoring force, and often use fin stabilizers to balance the pitching moment. However, fin stabilizers also bring additional drag (E. Begovic *et al*., 2015). For SWATH, the underwater pontoon resistance mainly accounts for the total resistance. Although many studies use computational fluid dynamics to analyze the pontoon resistance, a parametric method for pontoon design has yet to be proposed (F. Pérez-Arribas *et al*., 2020).

Although the computational of hardware has dramatically improved in recent years, free surface simulations still require relatively lengthy time. To reduce computational time, deep learning has been widely used in ship design and ocean engineering. There are many deep learning models, such as Recurrent Neural Networks (RNNs), Convolutional Neural Networks (CNNs), and Deep Neural Networks (DNNs), where the last group

uses a classic feedforward network. Since the design parameters of the ship form are neither time-series data nor two-dimensional matrix data, DNN is selected as the deep learning model in this study.

This study aims to propose a parametric design approach for optimizing SWATH vessel pontoon through minimizing the resistance and moment of the pontoon and fin stabilizers. In addition, this study also applies deep neural network technology to find an optimized ship form design.

2. PARAMETRIC DESIGN OF SWATH

2.1 Baseline Design

An existing SWATH vessel is used as the baseline design, where the displacement is 120 tons. Figure 1 shows its side view, and Table 1 lists the principal dimensions of the baseline design.

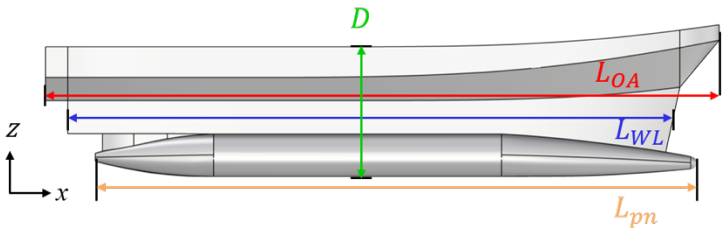

Figure 1. Side View of Baseline Design

Table 1. Principal Dimensions of the Baseline Design

L_{OA}	D	L_{WL}	L_{pn}
26 m	5.0 m	23.4 m	23.2 m

2.2 Resistance Calculation

To avoid the excessive computational cost of the free surface simulations, a simplified approach is used in this study.

$$R_T = R_{st}(Fr) + R_L(Re) \tag{1}$$

where, R_T is the total resistance, $R_{st}(Fr)$ is the strut resistance, and $R_L(Re)$ is the resistance of the lower hull. R_{st} is assumed a function of the Froude number only, while R_L is assumed a function of the Reynolds number. Furthermore, the resistance of the lower hull R_L can be further decomposed into two components as follows:

$$R_T = R_{st}(Fr) + R_{pn}(Re) + R_{fin}(Re) \tag{2}$$

where R_{pn} is the pontoon resistance, and R_{fin} is the fin stabilizer resistance. Figure 2 shows the variation of the pontoon resistance R_{pn} alongside its pressure and shear components with draught (d). The ratio of the pontoon resistance at the draught d, R_{pn}, to the pontoon resistance in the fully submerged case, R_{pn}^{∞}, is defined as β. The total resistance can be represented as follows:

$$R_T = R_{st}(Fr) + R_{pn}^{\infty}(Re) \cdot \beta(d) + R_{fin}(Re) \tag{3}$$

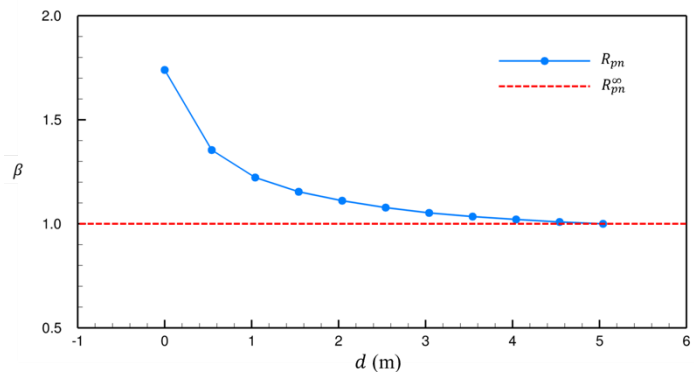

Figure 2. Pontoon Resistance vs. Draught

2.3 Design Parameters of Pontoon

This study proposes a parametric approach to design the pontoon by considering the pontoon as an axisymmetric body. The design length of the pontoon is 22.5 m. The pontoon is defined by four independent parameters that are the fore body length (L_f), the aft body length (L_a), the angle of entrance (θ_{pn}), and the angle of run (ϕ_{pn}). Figure 3 illustrates the design parameters of the pontoon, where R_h is the hub radius. L_f and L_a are limited between 1.8 m and 7.8 m, and θ_{pn} and ϕ_{pn} are limited between 10 degrees and 60 degrees.

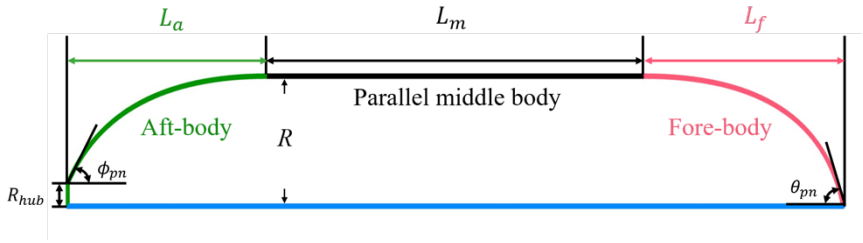

Figure 3. Design Parameters of Pontoon

2.4 Fin Stabilizer

Because pontoons are unable to deliver longitudinal stability, fin stabilizers are necessary (D. Vieira *et al.*, 2010). Fin stabilizers provide the lift force to keep the ship in an even keel position, especially at high speeds. Figure 4 schematically shows the position of fin stabilizers and the lift provided by the fore and aft fin stabilizers to balance the longitudinal moment of the SWATH vessel, where M_{hull} is the pitch moment contributed by ship hull, and M_{fin} is the pitch moment contributed by fin stabilizers. Figure 5 shows the aspect ratios of the fore and aft fin stabilizers, which are 0.668 and 0.689, respectively. However, lift also accompanies drag, as shown in Figure 6, where the slope of the ideal 2D lift curve is 2π (O.G. Tietjens *et al.*, 1957). As the angle of attack increases, the drag increases accordingly. If the pitch angle is too large, the angle of attack of the fin stabilizers must increase to balance the moment. Two foils, i.e., NACA0015 and NACA0030, are used for the aft and fore fin stabilizers, respectively.

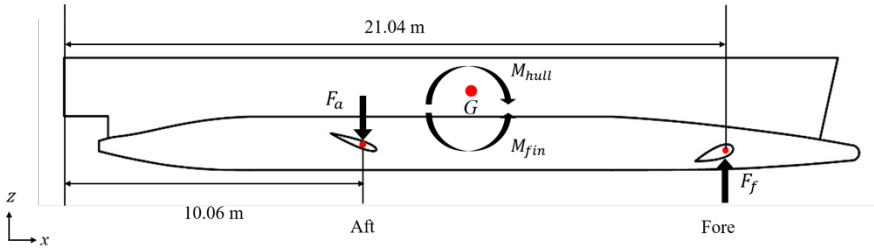

Figure 4. Position and Working Principal of Fin Stabilizers

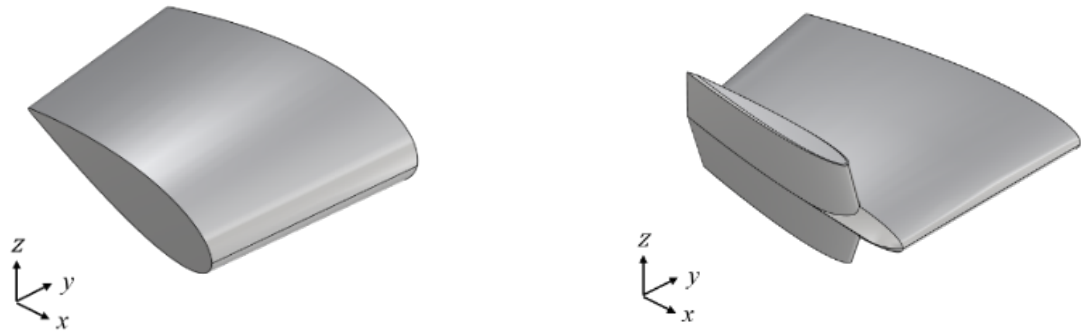

(a) (b)

Figure 5. Fin Stabilizer: (a) fore, (b) aft

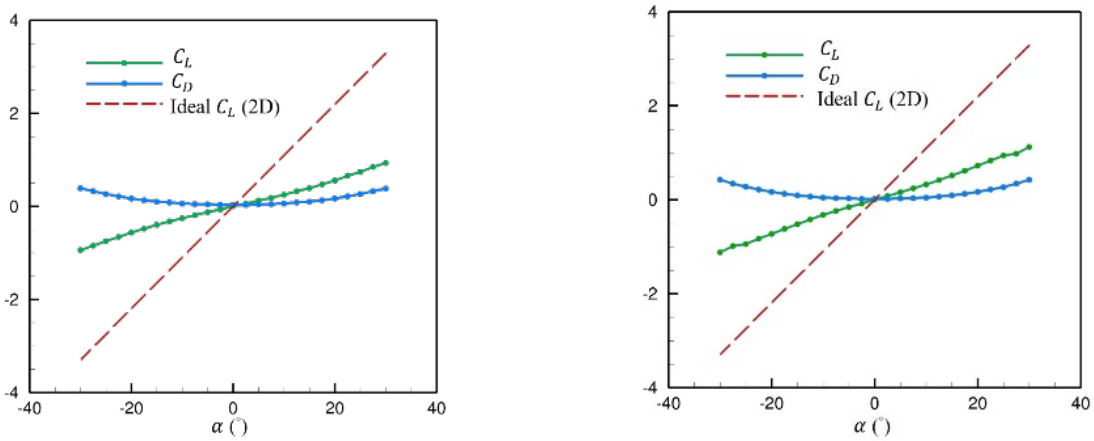

(a) (b)

Figure 6. Lift and Drag Coefficient of Fin Stabilizer: (a) fore, (b) aft

3. FLOW SOLVER

3.1 Governing Equations

This study uses the CFD software STAR-CCM+ to simulate the underwater pontoon's flow field and the full SWATH, where a finite volume method is used to discretize the governing equations. This study mainly optimizes the pontoon resistance under an immersed condition.

3.1.1 Pontoon Flow

The pontoon flow is assumed steady and incompressible. The governing equations are the continuity and momentum equations, and the $K-\epsilon$ turbulence model is to consider the turbulence effect.

$$\frac{\partial(\rho u)}{\partial z}+\frac{1}{r}\frac{\partial(\rho r v)}{\partial r}=0, \tag{4}$$

$$\frac{\partial(\rho u u)}{\partial z}+\frac{1}{r}\frac{\partial(\rho r u v)}{\partial r}=-\frac{\partial p}{\partial z}+\frac{\partial \tau_{zz}}{\partial z}+\frac{1}{r}\frac{\partial(r\tau_{zr})}{\partial r}, \tag{5}$$

$$\frac{\partial(\rho uv)}{\partial z}+\frac{1}{r}\frac{\partial(\rho rvv)}{\partial r}=-\frac{\partial p}{\partial r}+\frac{\partial \tau_{rz}}{\partial z}+\frac{1}{r}\frac{\partial(r\tau_{rr})}{\partial r}, \tag{6}$$

$$\frac{\partial(\rho uK)}{\partial z}+\frac{\partial(\rho vK)}{\partial r}=G-\rho\varepsilon+\frac{\partial}{\partial z}\left[\left(\mu+\frac{\mu_t}{\sigma_k}\right)\frac{\partial K}{\partial z}\right]+\frac{1}{r}\frac{\partial}{\partial r}[r\left(\mu+\frac{\mu_t}{\sigma_k}\right)\frac{\partial K}{\partial r}], \tag{7}$$

$$\frac{\partial(\rho u\varepsilon)}{\partial z}+\frac{\partial(\rho v\varepsilon)}{\partial r}=c_{\varepsilon 1}G\frac{\varepsilon}{K}-c_{\varepsilon 2}G\frac{\varepsilon^2}{K}+\frac{\partial}{\partial z}\left[\left(\mu+\frac{\mu_t}{\sigma_\varepsilon}\right)\frac{\partial \varepsilon}{\partial z}\right]+\frac{1}{r}\frac{\partial}{\partial r}\left[r\left(\mu+\frac{\mu_t}{\sigma_\varepsilon}\right)\frac{\partial \varepsilon}{\partial r}\right], \tag{8}$$

where ρ is the fluid density, u and v represent the velocity component in z and r direction, respectively, p is the pressure of the flow field, μ is the dynamic viscosity, G is the production term of the kinetic energy of turbulence, μ_t is the turbulent dynamic viscosity, $\dot{\gamma}$ is the shear rate, and c_μ, σ_K, $c_{\varepsilon 1}$, $c_{\varepsilon 2}$, σ_ε are the equation constants of the $K-\epsilon$ turbulence model.

3.1.2 Free Surface Ship Flow

The governing equations used to simulate the free surface flow are the continuity equation and momentum equations, where the fluid is assumed incompressible.

$$\frac{\partial U_i}{\partial x_i}=0, \tag{9}$$

$$\frac{\partial U_i}{\partial t}+\frac{\partial\left(U_iU_j\right)}{\partial x_j}=-\frac{1}{\rho}\frac{\partial p}{\partial x_i}+\frac{\partial}{\partial x_j}\left[\nu\left(\frac{\partial U_i}{\partial x_j}+\frac{\partial U_j}{\partial x_i}\right)\right]-\frac{\partial\overline{\left(u_i'u_j'\right)}}{\partial x_j}, \tag{10}$$

where U_i and u_i' are the mean velocity and fluctuation of velocity in x_i direction, respectively, ν is the kinematic viscosity, and $\overline{\rho u_i'u_j'}$ is the Reynold's stress. The $K-\epsilon$ turbulence model is given as follows:

$$\frac{\partial U_i}{\partial t}+\frac{\partial\left(U_iU_j\right)}{\partial x_j}=-\frac{1}{\rho}\frac{\partial p}{\partial x_i}+\frac{\partial}{\partial x_j}\left[\nu\left(\frac{\partial U_i}{\partial x_j}+\frac{\partial U_j}{\partial x_i}\right)\right]-\frac{\partial\overline{\left(u_i'u_j'\right)}}{\partial x_j}, \tag{11}$$

$$\frac{\partial \varepsilon}{\partial t}+\frac{\partial\left(KU_j\right)}{\partial x_j}=\frac{\partial}{\partial x_j}\left[\left(\nu+\frac{\nu_t}{\sigma_\varepsilon}\right)\frac{\partial \varepsilon}{\partial x_j}\right]+C_{\varepsilon 1}G_k\frac{\varepsilon}{\rho K}-C_{\varepsilon 2}\frac{\varepsilon^2}{K}, \tag{12}$$

where G_k is the production term of the kinetic energy of turbulence. To describe the free surface, a volume of fluid method is used. The volume fraction of fluid in a cell can be expressed as

$$C_a=\frac{V_a}{V},\ C_w=\frac{V_w}{V}, \tag{13}$$

where V_a is the air volume, V_w is the water volume, and V is the total volume. The sum of all the volume fractions in a cell is unity, as (14):

$$C_a+C_w=1. \tag{14}$$

$C_a=0$ indicates that the cell does not contain air; $C_a=1$ indicates that the cell is filled with air; $0<C_a<1$ indicates a free surface existing in a cell. This study defines $C_a=0.5$ as the location of the free surface. The fluid density and the dynamic viscosity are defined as follows:

$$\rho=\rho_aC_a+\rho_wC_w, \tag{15}$$

$$\mu = \mu_a C_a + \mu_w C_w, \tag{16}$$

where the subscript a and w represent air and water, respectively. The free surface equation is given as follows:

$$\frac{\partial C_a}{\partial t} + U_k \frac{\partial C_a}{\partial x_k} + \nabla \cdot \left(C_a U_{d,a}\right) + \nabla \cdot \left(C_a(1 - C_a) U_{c,a}\right) = 0, \tag{17}$$

where $U_{d,a}$ and $U_{c,a}$ represents the diffusion rate and the boundary sharpening speed, respectively.

3.2 Computational Domain and Boundary Conditions

3.2.1 Pontoon Flow

Figure 7 shows the computational domain for axisymmetric flows. Table 2 lists the dimensions and boundary conditions of the computational domain, where u_s is the ship speed. The inflow boundary is L_{pn} measured from the bow, and the pressure outflow boundary is 2.0 L_{pn} measured from the stern. The radius of the computational domain is L_{pn}, where $L_{pn}$is 22.5 m.

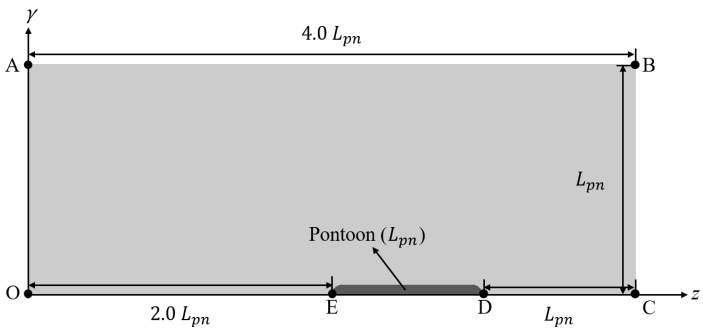

Figure 7. Computational Domain of Pontoon Flow

Table 2. Dimensions and Boundary Conditions of Pontoon Flow

Region	L_{pn}	Boundary Condition
$\overline{\text{AB}}$	4.0	$\mathbf{U} = (-u_s, 0)$
$\overline{\text{BC}}$	1.0	
$\overline{\text{OA}}$	1.0	$p = 0$
$\overline{\text{CD}}$	1.0	$\mathbf{U} = (u, v)$
$\overline{\text{EO}}$	2.0	$\frac{\partial \mathbf{U}}{\partial \text{n}} = 0$
$\overline{\text{DE}}$	1.0	$\mathbf{U} = 0$

3.2.2 Free Surface Ship Flow

Figure 8 shows the computational domain for the free surface case. Since the ship has a starboard-portside symmetry, only half of the ship hull is considered in the simulation to reduce computational cost. The inflow boundary is 1.5 L_{pn} away from the bow, and the pressure outflow boundary is 3.5 L_{pn} away from the stern. The width and depth of the domain are both 1.5 L_{pn}. Table 3 summarizes the adopted boundary conditions.

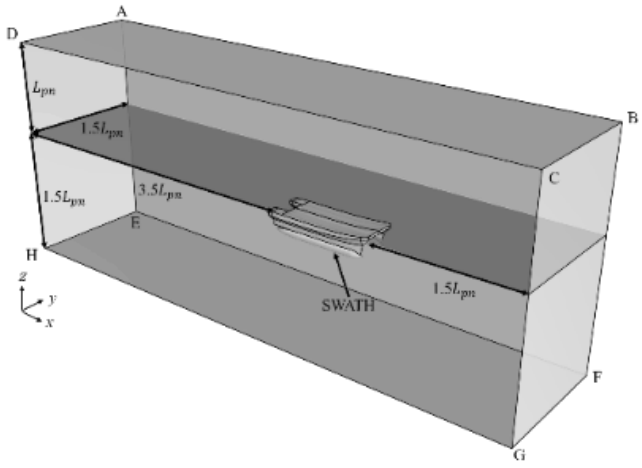

Figure 8. Computational Domain of Ship Flow

Table 3. Boundary Conditions of Ship Flow

Region	Boundary Condition
ABCD	$\mathbf{U} = (-u_s, 0, 0)$
BFGC	
ABFE	
EFGH	
AEDH	$p = p_s(Z)$
DCGH	$\frac{\partial \mathbf{U}}{\partial \mathbf{n}} = 0$
SWATH	$\mathbf{U} = 0$

4. DEEP NEURAL NETWORKS

4.1 Structures of DNN Model

Deep neural networks (DNNs) consist of input, hidden, and output layers. In a DNN model, the input value n_i is first introduced into the input layer, then multiplied by various weights and summed with biases in the hidden layer neurons before being passed through an activation function to become the input for the next layer. This process is called forward propagation and is represented by (18) and (19).

$$m_j^{hl} = T\left(w_{ij}^{hl} n_i + b_j^{hl}\right), \tag{18}$$

$$y_k^p = P\left(w_{jk}^{ol} m_j^{hl} + b_k^{ol}\right), \tag{19}$$

where w_{ij}^{hl} is the weight of the hidden layer, b_j^{hl} is the bias of the hidden layer, w_{jk}^{ol} is the weight of the output layer, b_k^{ol} is the bias of the output layer, n_i and y_k^p represent the ith input and kth output, respectively. The subscript i corresponds to the ith input, j to the jth node, and k to the kth output. The transfer function T is the Tansig function, and P is the Purelin function. The predicted value y_k^p of the neural network is then compared with the actual value y_k^a in the data to obtain the mean squared error e, which can be represented by (20).

$$e = \sum_{k=1}^{r} \left(y_k^a - y_k^p\right)^2, \tag{20}$$

where r represents the number of inputs and outputs. The mean squared error is then passed back to the previous layer, and the weights and biases are recalculated to obtain a new error. This process is repeated several times until the mean squared error between y_k^a and y_k^p approaches zero. This process is called backpropagation, and Bayesian regularized backpropagation is used in this study.

4.2 Parameters of DNN Model

In this study, a deep neural network model is trained using MATLAB, which consists of one input layer, five hidden layers, and one output layer. Each hidden layer contains eight, six, nine, five, and seven neurons, respectively. The structure of the DNN model is shown in Figure 9. After the model is trained, a specific range

of design parameters is selected and the pontoons are extracted at intervals to predict the resistance. The parameter ranges are listed in Table 4.

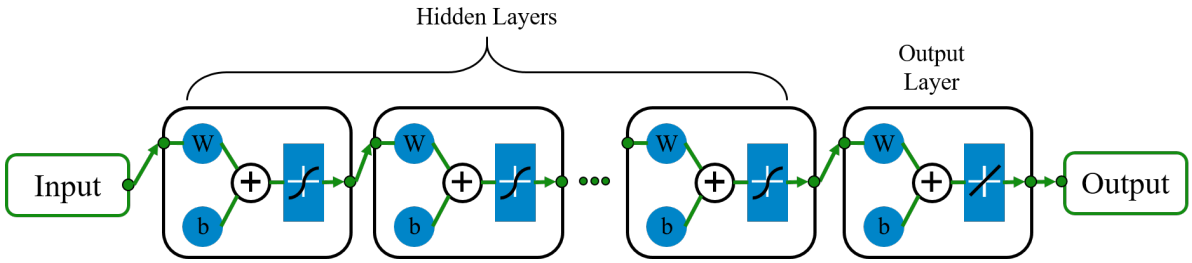

Figure 9. Schematic Illustration of The Employed DNN Model

Table 4. Pontoon range

	L_f (m)	L_a (m)	θ_{pn} (°)	ϕ_{pn} (°)
Upper Limit	1	4	10	10
Lower Limit	4	8	90	90
No. of Intervals	7	8	10	10

4.3 Result of Trained DNN Model

This study uses the mean absolute percentage error (MAPE) as the loss function to train about 1400 cases where 80 cases are used as the test data.

$$\text{MAPE} = \frac{1}{r}\sum_{i=1}^{r}\left|\frac{y_k^a - y_k^p}{y_k^a}\right|. \tag{21}$$

The MAPE of the training data and test data are 0.21% and 0.38%, respectively. Figure 10 shows the scatter plot of the actual values versus predicted values, where each red dot represents a case. The closer the dot to the black line is, the more accurate the predicted value is. Because the MAPE is smaller than 1%, the proposed model is considered accurate enough.

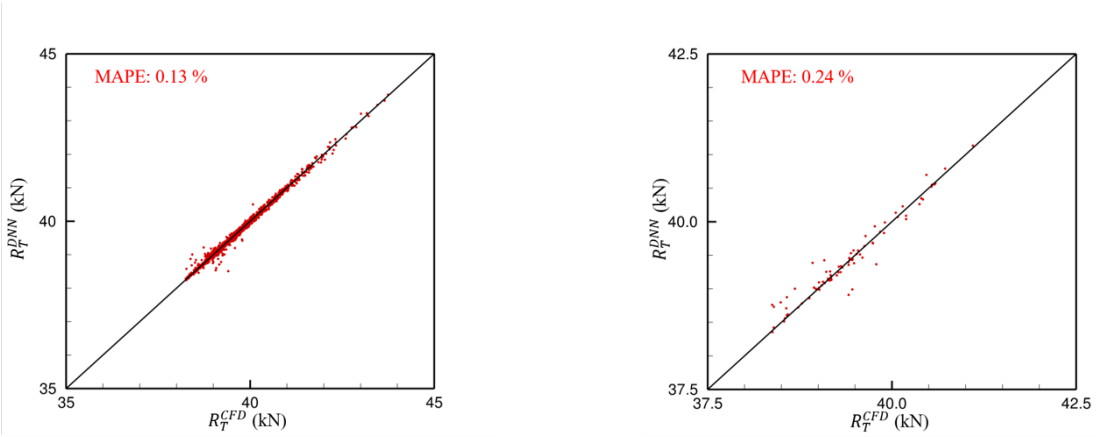

Figure 10. MAPE of DNN Model: (a) Training data, (b) Test data

5. RESULTS AND DISCUSSION

5.1 CFD Validation

In this study, the optimized pontoon parameters predicted by the DNN model are validated using a full CFD computation. Table 5 compares the geometric parameters between two hull forms. The optimized pontoon has a longer fore-body and a much shorter aft-body. Figure 11 shows the optimized shape provides a better pressure distribution than that of the baseline design to produce a much smaller longitudinal moment and resistance. Table 6 shows the resistance and moment of the pontoon, where R_T^{DNN} is predicted by the DNN model, R_T^{CFD} is predicted by a three-dimensional free surface ship flow, M_{pn} is the longitudinal moment of the pontoon, α_1 and α_2 represent the angle of attack of the fore and aft fin stabilizers, respectively, and θ represents the pitch angle. α_1 and α_2 of the optimized hull form are much smaller than those of the baseline design, indicating that the fin stabilizer drag of the optimized hull is smaller. The validation indicates that the DNN model is capable of predicting an optimal set of geometric parameters for a pontoon. However, some resistance prediction error arises due to decoupling the pontoon from the full hull form in the resistance calculation.

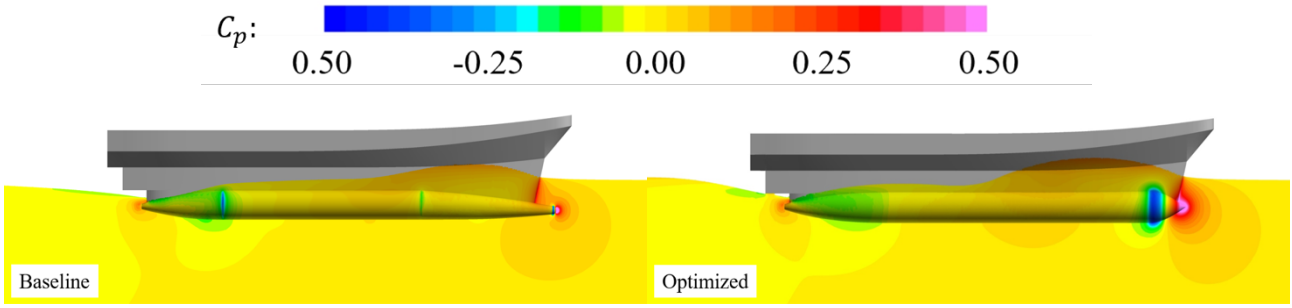

(a) (b)

Figure 11. Pressure distribution on the pontoon surface: (a) Baseline Design, (b) Optimized Design

Table 5. Geometric Parameters of Optimized and Baseline Design

Hull Form	L_f (m)	L_m (m)	L_a (m)	θ_{pn} (˚)	ϕ_{pn} (˚)
Baseline	7.54	11.12	4.56	N/A	N/A
Optimized	2.00	14.79	5.71	36.67	18.88

Table 6. CFD Validation

Hull Form	α_1 (˚)	α_2 (˚)	R_T^{DNN} (kN)	R_T^{CFD} (kN)	M_{pn} (kN·m)
Baseline	12.49	-12.49	88.54	116.88	446.97
Optimized	3.76	-3.76	76.30	102.83	39.39

CONCLUSIONS

This study aims to optimize the calm water resistance of a 120-ton SWATH vessel at a speed of 24 knots while maintaining an even keel using fin stabilizers. This study neglects the resistance interaction between the pontoon and the ship hull to reduce computational cost and time. Approximately 1400 cases using four hull form parameters are used to train a deep neural network model using MATLAB, and the MAPE is used as the loss function This study demonstrates that the optimized hull form reduces the total hull resistance by approximately 12.8% compared to the baseline design. The optimized design is L_f of 2 m, L_a of 5.71 m, θ_{pn} of 37°, and ϕ_{pn} of 19°. The optimized design has a smaller pitch moment because of the favorable pressure distribution due to the pontoon shape. The result shows that the optimized design has a smaller pitch moment as well as a substantially smaller total resistance.

REFERENCES

D. Vieira, et al., "Parametric Comfort Analysis of a Standard Swath Vessel", in International Conference on Offshore Mechanics and Arctic Engineering, pp. 67-74, 2010.

E. Begovic, C. Bertorello, and S. Mancini, "Hydrodynamic performances of small size swath craft," Brodogradnja, Vol. 66, pp. 1-22, 2015.

F. Pérez-Arribas and J. Calderon-Sanchez, "A parametric methodology for the preliminary design of SWATH hulls," Ocean Engineering, Vol. 197, 2020, Art no. 106823.

GWEC, "Global Wind Report," 2021. [Online]. Available: https://gwec.net/wp-content/uploads/2021/03/GWEC-Global-Wind-Report-2021.pdf

O.G. Tietjens and L. Prandtl. (1957). Fundamentals of hydro and aeromechanics; based on lectures.

S. Brizzolara, et al., "Hydrodynamic Design of a Family of Hybrid SWATH Unmanned Surface Vehicles," in 11th International Conference on Fast Sea Transportation, 2011.

Y. Dalgic, I. Lazakis, and O. Turan, "Investigation of Optimum Crew Transfer Vessel Fleet for Offshore Wind Farm Maintenance Operations," Wind Engineering, Vol. 39, pp. 31-52, 2015.